International Journal of Mechanical, Industrial and Aerospace Sciences
ISSN: 2517-9950
Vol:6, No:3, 2012

Strength Optimization of Induction Hardened Splined Shaft – Material and Geometric Aspects

I. Barsoum and F. Khan

***Abstract*—**the current study presents a modeling framework to determine the torsion strength of an induction hardened splined shaft by considering geometry and material aspects with the aim to optimize the static torsion strength by selection of spline geometry and hardness depth. Six different spline geometries and seven different hardness profiles including non-hardened and through-hardened shafts have been considered. The results reveal that the torque that causes initial yielding of the induction hardened splined shaft is strongly dependent on the hardness depth and the geometry of the spline teeth. Guidelines for selection of the appropriate hardness depth and spline geometry are given such that an optimum static torsion strength of the component can be achieved.

***Keywords*—**Static strength; Splined shaft; Torsion; Induction hardening; Hardness profile; Finite Element; Optimization; Design.

I. Introduction

THERE is an increased demand on power handling capacity of automotive transmission parts requiring high static and fatigue strength. Especially in splined shafts transferring high torque commonly used in heavy trucks, the choice of spline geometry and heat treatment process is crucial in obtaining an adequate strength of the component. For such connections yielding or ultimate fracture are potential modes of failure, particularly when overloads are involved. Since hardness of the material is strongly related to the strength of the material a common method of heat treatment of splined shafts is induction hardening, which increases the torque capacity of the shaft. Along with the material aspects associated with the heat treatment process, the strength of a spline connection is also dependent upon the geometrical design of the spline. Involute splines are commonly used in automotive industry with profiles similar to those of involute gear teeth. In the past, several studies [1-4] have focused on the failure analysis and failure prevention of splined or non-splined shafts; however none have attempted to quantify the simultaneous effect of the spline geometry and the hardness profile and depth on the torsion strength.

The objective of this study is to develop a modeling framework such that to quantify the increase in torsion strength of a splined shaft with respect to the geometry of the spline and the hardness profile and hardness depth due to the induction hardening process.

I. B. Author is a faculty at the Department of Mechanical Engineering, the Petroleum Institute, Abu Dhabi, UAE (e-mail: ibarsoum@pi.ac.ae).

F. K. Author is a graduate student at the Department of Mechanical Engineering, the Petroleum Institute, Abu Dhabi, UAE (e-mail: fkhan@pi.ac.ae).

II. Geometry of the Involute Spline

There are various international standards in which a thorough definition of the spline geometry can be found [5-7]. Here the geometry of the involute spline and the geometric quantities that define the spline will be briefly described. The terminology of a involute splined shaft is shown in Fig. 1. The pitch circle with radius r_p is the theoretical circle upon which several geometric parameters are defined such as the pressure angle α. The number of spline teeth is denoted Z which together with r_p defines the module m of the spline as

$$m = 2r_p / Z \tag{1}$$

which is an indication on the size of the spline tooth. The top and bottom land of the tooth are defined by the addendum radius r_a and the dedendum radius r_d, respectively.

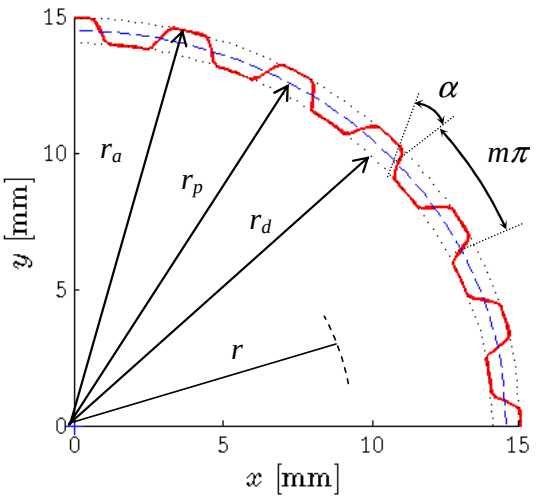

Fig. 1 Parameters defining the spline geometry

In the present study six different spline geometries where considered comprising of two different pressure angles α = 30° and 45° and three different tooth numbers Z = 20, 30 and 40. Based on the polar moment of inertia of a circular shaft the static torsional yield strength scales with the cube of the spline dedendum radius ($\propto r_d^3$). Therefore the addendum radius r_a of the spline has been kept fixed while the dedendum radius r_d is varied by changing the module m of the spline as. Consequently the pitch radius r_p is given by Eq. (1) once the module m is set. The values of the module considered here are m = 0.73, 0.97 and 1.44 mm.

III. Mechanical Properties of 42CrMoS4

The material considered in the shaft is an induction hardened medium carbon steel denoted 42CrMoS4, which is commonly used in transmission components and drive shafts in the automotive industry. By varying the process parameters in the induction hardening process various hardness depths and profiles can be achieved. Mechanical properties such as yield and ultimate strength are closely related to the hardness where the yield strength is approximately one third of the hardness in HV (Vicker's hardness). In Fig. 2(a) the stress-strain curves show that the work-hardening behavior as well as the yield and ultimate strength strongly depend on the hardness level where each stress-strain curve correspond to a hardness value. Given the chemical composition of 42CrMoS4 the stress-strain behavior can be determined with the materials simulation software JMATpro® [8]. Also the yield and ultimate strength for each hardness value can be obtained as shown in Fig. 2(a). The stress-strain curves can be fitted to the plasticity model given by

$$\varepsilon = \frac{\sigma}{E} + \left(\frac{\sigma}{K}\right)^N \tag{2}$$

where E = 200 GPa is the elastic modulus, K the plastic modulus and N the hardening exponent respectively. Hence, the yield strength R_{p02}, the ultimate strength R_m and the plasticity model parameters K and N can be obtained as function of Vickers hardness H as shown in Fig. 2(b)-(c). The plasticity model parameters K and N as function of hardness H are given by Eq. (3) and (4).

$$N = n_0 e^{n_1 H} \tag{3}$$

$$K = k_0 H + k_1 \tag{4}$$

The constants in Eq. (3) and (4) are: n_0 = 0.4911, n_1 = 0.00232 1/HV, k_0 = 0.0034 MPa/HV and k_1 = 0.3 MPa. Now, for a specific hardness value given in HV the stress-strain behavior can be determined from Eq. (2)-(4) which in combination with the hardness profile of the induction hardened shaft gives the gradient in mechanical behavior of the shaft.

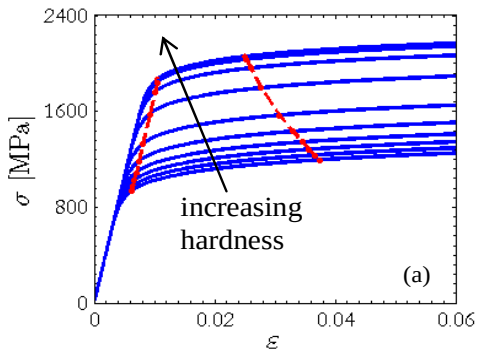

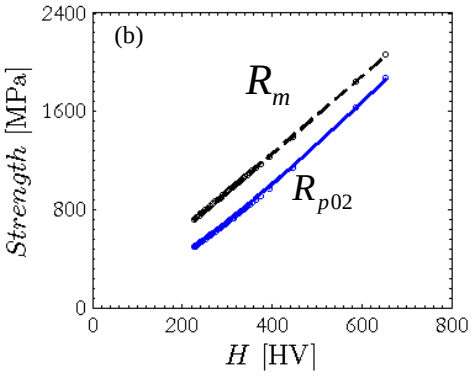

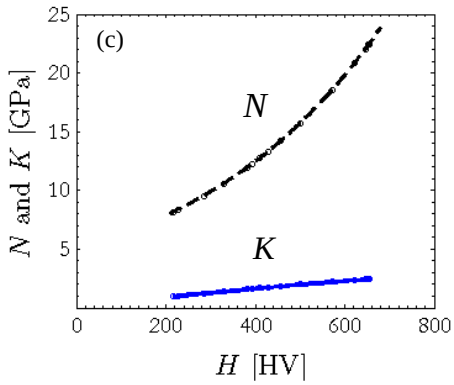

Fig. 2 Mechanical properties of 42rMoS4

IV. Hardness Profile and Depth

Fig. 3(a) shows measured hardness H in HV against depth below surface (1 - r) (c.f. Fig. 1) of an induction hardened shaft. It is notable that the hardness is highest at the outer surface 630 HV and decreases towards the center of the shaft reaching the value of the core hardness 230 HV. To quantify the depth of the hardness most often a hardness depth is defined. Here the hardness depth D_H is defined as the depth below the surface at which the hardness level reaches a value of 400 HV. For the case shown in Fig. 3(a) D_H = 5 mm, which is about 30% of the shaft radius. In a similar manner as in [9] the hardness profile can be described as a function of the depth below the surface (1 - r) by the function

$$H(r) = H_{case}\, g(r) + H_{core}\left(1 - g(r)\right) \tag{5}$$

where H_{case} = 630 HV, H_{core} = 230 HV and the function $g(r)$ is given by

$$g(r) = \begin{cases} 1 & r \le r_1 \\ 1 + c_1\left(\frac{r - r_1}{r_2}\right)^2 + c_2\left(\frac{r - r_1}{r_2}\right)^3 & r_1 < r \le r_2 \\ 0 & r > r_2 \end{cases} \tag{6}$$

Some restrictions on $g(r)$ and $H(r)$ are: $\partial g(r_1)/\partial r = g(r_1) = g(r_2) = 0$ and $H(r{=}1{-}D_H) = 400$. For a given value of the hardness depth D_H this will yield four equations which are

solved for the four unknowns c_1, c_2, r_1 and r_2. By varying the hardness depth D_H different hardness profiles can be achieved with Eqs. (5) and (6). As shown in Fig. 3(b) five different hardness depths were considered in this study with D_H = 2.5, 5.0, 6.0, 7.0 and 8.0 mm. Additional two hardness depths values were considered, D_H = 0 and D_H = ∞, corresponding to a non-hardened shaft with a uniform hardness of 230 HV and through-hardened shaft with a uniform hardness of 630 HV.

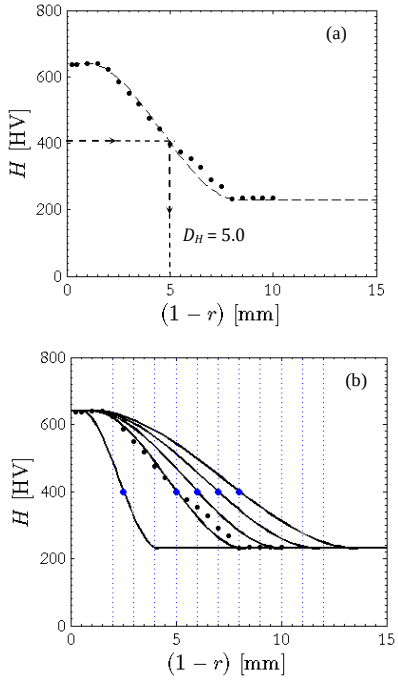

Fig. 3 (a) Measured hardness profile of a splined shaft and (b) hardness profiles given by Eqn. (5)

V. The Finite Element Model

In order to determine the static strength in torsion of an induction hardened shaft accounting for the effect of spline geometry (Fig. 1) and hardness depth (Fig. 3(b)) a 3D finite element model was built using the commercial package ABAQUS [10]. Since the geometry and torsion loading exhibits cyclic symmetry, only one tooth of the splined shaft along with the corresponding cyclic symmetric segment of the hub was modeled as shown in Fig. 4. The back faces of the hub as well as that of the spline are kinematic ally coupled to reference points. The reference point of the hub is given an encastred displacement boundary condition whereas the reference point of the shaft is given a concentrated torque T. A contact definition is established between the hub and spline surfaces that are in contact with a friction coefficient of 0.1. The hub is modeled as an elastic material (E = 210 GPa and ν = 0.3) whereas the spline is modeled as elastic-plastic material with isotropic hardening. The splined shaft is sliced into 13 different layers radially with the non-hardened core layer at the center and the case with highest hardness at the outer layer. Depending on the hardness depth D_H analyzed each layer in Fig. 4 will have different hardness values due to the varying hardness profile as function of hardness depth D_H (cf. Fig. 3(b)). Consequently, since the plastic behavior is linked to the hardness by Eq. (2)-(4), each layer in the model will be assigned an elastic-plastic true stress-strain curve corresponding to its hardness value following the hardness profile given by D_H. The finite element mesh used consisted of about 26 000 eight-node continuum elements.

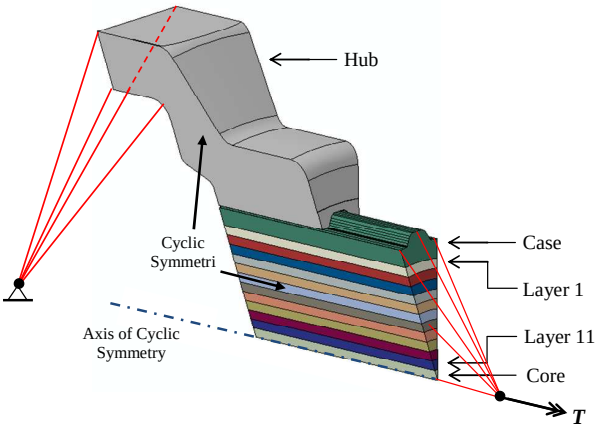

Fig. 4 The cyclic symmetric FEM model

VI. Results

The results from the finite element models are generated for six different geometries of the spline on the shaft comprising of three different number of teeth (Z = 20, 30, 40) and two different pressure angles (α = 30°, 45°) with seven different hardness depths values D_H = 0, 2.0, 5.0, 6.0, 7.0, 8.0 and ∞, summing up to a total of 42 different models. For each run the torque T and the end twist of the shaft is monitored, from which the corresponding shear strain γ can be calculated. In Fig. 5 the torque T versus the shear strain γ is plotted, which pertains to results with α = 30°, all Z and D_H values. As the figure reveals the hardness depth has a strong effect on the T vs. γ behavior of the shaft. Also the number of spline teeth Z affects the level of static torque the shaft can carry. However, it was further found that the pressure angle α has a very minor influence on the torsion strength and hence the results for α = 45° are not reported here.

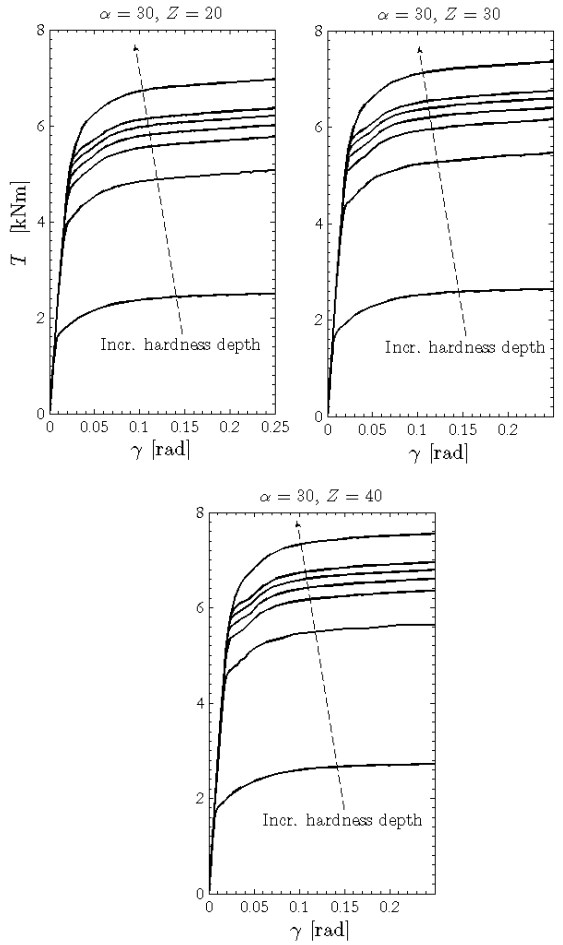

Fig. 5 Torque T versus shear strain γ for pressure angle α = 30°, various spline teeth Z and hardness depth D_H

VII. Conclusion

The current study presents a finite element modeling framework to obtain the torsion strength of an induction hardened splined shaft by considering both the geometrical and material aspects in the model. It can be concluded by comparing the different plots in Fig. 5 that increasing the number of teeth Z, which corresponds to increasing the dedendum radius rd and keeping the addendum radius r_a constant, increases the torsion strength of the shaft. The largest contribution to the increase in torsion strength is however due to the increase in hardness depth D_H as evidenced from Fig. 5, where the non-hardened shaft (lowest D_H) has the lowest strength while the through hardened shaft (highest D_H) has the maximum strength. Additionally, it is found that the pressure angle α has no marketable effect on the strength.

References

[1] "On the profile design of transmission splines and keys", C.H. Yanga, S.H. Tong, Mechanism and Machine Theory, Vol. 42, Issue 1, 2007, pp 82-87.
[2] "Fracture analysis of spline shaft", Hu.C. Yan, L.D. Lin, W. Fang, C.Hu. Tao, Journal of Materials Engineering, Vol. 5, pp. 57-59, 2009.
[3] "A combined testing and modelling approach to the prediction of the fretting fatigue performance of splined shafts", Journal of Aerospace Engineering, Vol. 215 (2), pp. 105-112, 2001.
[4] "Failure Analysis of Induction Hardened Automotive Axles", Journal of Failure Analysis and Prevention, Vol. 8 (4), pp. 386-396, 2008.
[5] ISO 4156-1:2005. Straight cylindrical involute splines – Metric module, side fit – Part 1: Generalities. 2005-10.
[6] DIN 5480-1. Involute splines based on reference diameters – Part 1: General. 2006-03.
[7] DIN 5480-2. Involute splines based on reference diameters – Part 2: Nominal and inspection dimensions. 2006-03.
[8] JMATpro 4.1, the Materials Property Simulation Package, Sente Softare Ltd.
[9] "Tooth interior fatigue fracture – computational and material aspects", M. MackAldener and M. Olsson, International Journal of Fatigue, Vol. 23, 2000, pp. 283-292.
[10] ABAQUS, 2009. Standard User's Manual, Version 6.9, Dassault Systèmes Simulia